MJFAS
Malaysian Journal of Fundamental and Applied Sciences

Jillani *et al.* | Malaysian Journal of Fundamental and Applied Sciences, Vol. 21 (2025) 2557–2575

RESEARCH ARTICLE

Investigating the Effect of Ligand Conjugation or Substituent in Ruthenium Complexes for Nonlinear Optical Application

Mamoona Jillani[a], Nur Hidayah Tahang[a], Nur Amira Mohd Yusuf[a], Suhaila Sapari[a], Yee Shi Wee[a], Fazira Ilyana Abdul Razak[a,b]*

[a]Department of Chemistry, Faculty of Science, Universiti Teknologi Malaysia, 81310, UTM Johor Bahru, Johor, Malaysia; [b]Department of Physics, Faculty of Science and Technology, Universitas Airlangga, Surabaya, Indonesia

Abstract Different nonlinear optic (NLO) properties can be achieved by incorporating various π-conjugated substituents with benzene and naphthalene in ruthenium complexes. To assess the NLO characteristics, a combination of experimental and computational approaches was employed to validate the gathered data. This research involved the synthesis of eight compounds, specifically four distinct diaminophosphine ligands (L1-L2) and their corresponding complexes (C1-C4). The synthesis process yielded a percentage range of 36-69%, and the compounds were subsequently characterized using techniques such as Fourier transform infrared spectroscopy (FTIR), ^{1}H and ^{31}P nuclear magnetic resonance (NMR), as well as ultraviolet-visible (UV-vis) spectroscopy. The experimental results were then compared to the theoretical calculations of FTIR, NMR, and UV-Vis spectroscopy to ensure data validation. In the computational aspect of the study, density functional theory (DFT) based on the B3LYP/6-31G(d,p) level was employed to investigate the NLO properties. The DFT method successfully optimized the geometry of the studied compounds with a deviation error ranging from 0.53% to 4.39% in terms of bond lengths and bond angles. By calculating the first hyperpolarizability, β_{tot}, at 1064 nm, it was determined that C3 exhibited a strong NLO property (6748.34 x 10^{-30} esu) according to the DFT analysis. This high NLO property can be attributed to the presence of an amine group, which acts as a potent electron-donating group (EDG). Furthermore, the calculation of the lowest HOMO-LUMO energy gap for C3 supported these findings and indicated its suitability as a prime candidate for NLO applications.

Keywords: Nonlinear optic, ruthenium complex, Density Functional Theory, ligand conjugation, diaminophosphine.

***For correspondence:**
fazirailyana@utm.my

Received: 17 Feb. 2025
Accepted: 13 August 2025

Introduction

Schiff base was first described by Hugo Schiff in 1864. A Schiff base is an organic compound containing an azomethine group (-HC=N) that results from the condensation of ketones or aldehydes with primary amines. Compared to aliphatic aldehydes, aromatic aldehydes with a conjugation system create a more stable Schiff base, and when functioning as a Schiff-based ligand, it produces exceptionally stable complexes with metal ions [1]. Due to their use in a variety of domains, including biology, chemistry, and physics, Schiff base ligands are a significant class of organic molecules [2]. For nonlinear optical (NLO) materials, conjugated organic molecules with acceptor and donor groups on opposite sides of the molecule are key properties. The donor-(π electron bridges)-acceptor (D-π-A) structure has been successfully used in the development of second-order NLO metal complexes, where charge transfer occurs via metal-to-ligand (MLCT), ligand-to-metal (LMCT), or intraligand (ILCT) excitations. Therefore, organometallic groups can act as donor and/or acceptor groups in the D-π-A system [3].

Organometallic complexes are the most extensively studied NLO materials due to their optoelectronic properties. These properties rely heavily on the *d*-orbital of the metal and its energy levels, which can be manipulated by varying the type of metal, oxidation state, and surrounding ligands to optimise charge transfer interaction [4]. NLO phenomena involve non-linear responses like frequency modulation, polarisation, phase variation, and light incidence path alterations. One significant effect of these nonlinear interactions is second harmonic generation (SHG), which is connected to the frequency-dependent first hyperpolarizability, β_{tot} [5]. In the SHG process, two interacting photons at fundamental frequency "combined" effectively to produce new photons with a frequency that is twice as high of its input frequency. This process typically takes place in a nonlinear medium, such as crystals. For example, an Yttrium-Aluminium-Garnet (Nd:YAG) laser operating at 1064 nm can produce green light (532 nm) via frequency doubling [6].

The study of NLO properties and complex structures can be designed by using computational chemistry. Molecular geometry optimization provides insights into bond lengths, bond angles, and dihedrals. In addition, computational studies also provide valuable information on molecular energy levels, spectroscopic information, electronic transitions, and orbital interactions including the highest occupied molecular orbital (HOMO) and the lowest unoccupied molecular orbital (LUMO) energy gaps [7]. In this study, density functional theory (DFT) calculations were conducted using the B3LYP functionals and the 6-31G(d,p) basis set to examine molecular properties. The selected compounds for this study were designed based on the impact of ligand substituents, where one compound featured a cyclic substituent such as benzene, while another had an acyclic substituent such as propane. The NLO characteristics of these compounds with cyclic and acyclic substituents were investigated. Ruthenium was chosen as the metal due to its stability at room temperature, frequent application in NLO materials, and ability to donate electrons to ligands via MLCT due to its highly polarizable d-orbitals.

This research aims to synthesize and characterize four different diaminophosphine ligands, followed by synthesis and characterization of their corresponding ruthenium metal complexes. The study also aims to investigate the influence of ruthenium metal with diaminophosphine ligands on NLO properties through DFT calculations. The four synthesized ligands are:

- L1: *N,N'-bis*[2-(diphenylphosphino)benzylidene]cyclohexane-1,2-diamine.
- L2: *N,N'-bis*[2-(diphenylphosphino)benzylidene]propane-1,2-diamine.
- L3: *N,N'-bis*[2-(diphenylphosphino)benzylidene)phenyl-1,2-diamine.
- L4: *N,N'-bis*[2-(diphenylphosphino)benzylidene)naphthalene-1,8-diamine.

Materials and Methods

General Experimental Conditions and Starting Materials

All the chemicals used in this study were analytical grade (AR) with the highest purity available. All the solvents were used as received without further purification. The following were prepared according to the literature procedures: *N,N'-bis*[2-(diphenylphosphino)benzylidene]cyclohexane-1,2-diamine (L1) [8], *N,N'*-bis[2-(diphenylphosphino)benzylidene]propane-1,2-diamine (L2) [8], *N,N-bis*(2-(diphenylphosphino)benzylidene)phenyl-1,2-diamine (L3) [9], *N,N-bis*(2-(diphenylphosphino)benzylidene)naphthalene-1,8-diamine (L4) [9], *N,N'-bis*[2-(diphenylphosphino) benzylidene]cyclohexane-1,2-diamine dichlororuthenium (C1) [8], *N,N'-bis*[2-(diphenylphosphino)benzylidene]propane-1,2-diamine dichlororuthenium (C2) [8], *N,N'-bis*(2-(diphenylphosphino)benzylidene)phenyldiamine dichlororuthenium (C3) [9], and *N,N'-bis*(2-(diphenylphosphino)benzylidene)naphthalenediamine dichlororuthenium (C4) [9].

Instrumentation

The Agilent Cary 630 FTIR spectrometer with a resolution of 4.0 cm^{-1} was used to record the Fourier transform infrared (FTIR) spectrum of the investigated molecule. The samples were prepared as self-supporting pellets and analyzed in the range of 4000-400 cm^{-1} using a KBr window. The electronic absorption spectra were recorded using Shi-madzu UV-1800 UV/Visible spectrophotometer. ^{1}H and ^{31}P NMR spectra were recorded on a Bruker Advance (400 MHz) spectrophotometer.

Synthesis of (*N,N'-Bis*[2-(diphenylphosphino)benzylidene]cyclohexane-1,2-diamine Dichlororuthenium (C1)

A mixture of *N,N'-bis*[2-(diphenylphosphino)benzylidene]cyclohexane-1,2-diamine (0.10 g, 0.15 mmol) and $RuCl_2(DMSO)_4$ (0.07 g, 0.15 mmol) was dissolved in toluene (15 mL) and refluxed under stirring for

16 hours. The resulting brick-red solution was cooled to room temperature, and the solvent was removed under vacuum, leaving a brick-red residue. The solid was purified by column chromatography on silica using CH_2Cl_2/acetone (1:1) as eluent, yielding brick-red crystals. **Yield:** 50.87% (0.06 g). **^{1}H NMR** (400 MHz, $CDCl_3$) δ [ppm]: 8.67 (2H, d, -CH=N-), 6.87-7.98 (28H, m, ArH), 4.19 (2H, m, CH), 2.00-2.76 (4H, m, CH_2), 0.91-1.60 (4H, m, CH_2). **^{31}P NMR** ($CDCl_3$) δ [ppm]: 47.35. **FTIR** (KBr, cm^{-1}): 3412 m ν(CH)ar, 3050 s ν(HC=N), 2962 m, 2930 w ν(C-H), 1625 w ν(C=N), 1431 s ν(C=C)ar.

Synthesis of (*N,N'-Bis*[2-(diphenylphosphino)benzylidene]propane-1,2-diamine Dichlororuthenium (C2)

A mixture of *N,N'-bis*[2-(diphenylphosphino)benzylidene]propane-1,2-diamine (0.07 g, 0.15 mmol) and $RuCl_2(DMSO)_4$ (0.07 g, 0.15 mmol) was dissolved in toluene (7 mL) and refluxed under stirring for 16 hours. The resulting brick-red solution was cooled to room temperature, and the solvent was removed under vacuum to obtain a brick-red residue. The solid was purified by column chromatography on silica using CH_2Cl_2/acetone (1:1) as eluent, yielding brick-red crystals. **Yield:** 49.87% (0.06 g). **^{1}H NMR** (400 MHz, $CDCl_3$) δ [ppm]: 8.95, 8.75 (1H, d, -CH=N-), 6.59-7.63 (28H, m, ArH), 4.72 (2H, d, CH_2), 4.13-4.36 (1H, m, CH), 1.57 (3H, d, CH_3). **^{31}P NMR** ($CDCl_3$) δ [ppm]: 47.83. **FTIR** (KBr/cm^{-1}): 3140 w ν(CH)ar, 3051 s ν(HC=N), 2921 m, 2852 w ν(C-H), 1703 s ν(C=N), 1432 s ν(C=C)ar.

Synthesis of *N,N'-bis*(2-(diphenylphosphino)benzylidene)phenyldiamine Dichlororuthenium (C3)

A mixture of *N1,N2-bis*(2-(diphenylphosphino)benzylidene)phenyl-1,2-diamine (0.2 g, 0.3 mmol) and $RuCl_2(DMSO)_4$, (0.15 g, 0.3 mmol) was dissolved in toluene (15 ml) and refluxed under stirring for 16 hours. The resulting dark brown solution was cooled to room temperature, and the solvent was removed under vacuum, leaving a dark brown residue. The solid was purified by column chromatography using silica with a CH_2Cl_2/acetone (1:1) eluant, yielding dark brown crystals. **Yield:** 41.40%. **^{1}H NMR** (400 MHz, $CDCl_3$), δ [ppm]: 9.30 (2H, s, -HC=N-); 6.999-7.035 (4H, m, ArH); 7.159-7.600 (28H, m, ArH). **^{31}P NMR** ($CDCl_3$) δ [ppm]: 50.28. **FTIR** (KBr, cm^{-1}): 3055 m ν(CH)ar, 2923 w ν(HC=N), 1619 m ν(C=N), 1588 s ν(C=C)ar.

Synthesis of *N,N'-bis*(2-(diphenylphosphino)benzylidene)naphthalenediamine Dichlororuthenium (C4)

A mixture of *N1,N8-bis*(2-(diphenylphosphino)benzylidene)naphthalene-1,8-diamine (0.21 g, 0.3 mmol) and $RuCl_2(DMSO)_4$, (0.15 g, 0.3 mmol) was dissolved in methanol (15 ml) and refluxed under stirring for 16 hours. The resulting mixture was cooled to room temperature, and the solvent was removed under vacuum to obtain a solid residue. The solid was purified by column chromatography on silica using a CH_2Cl_2/acetone (1:1) eluant, yielding crystals. **Yield:** 51.48 %. **^{1}H NMR** (400 MHz, $CDCl_3$) δ [ppm]: 8.20 (2H, s, -CH=N-); 7.067-7.380 (6H, m, ArH); 7.489-7.692 (28H, m, ArH). **^{31}P NMR** ($CDCl_3$) δ [ppm]: 37.97. **FTIR** (KBr, cm^{-1}): 3294 m ν(CH)ar, 3054 m ν(HC=N), 1590 m ν(C=N), 1436 w ν(C=C) ar.

Computational Method

Computational studies were performed using a desktop computer with a 3.30 GHz CPU, a 64-bit operating system with a x64-based processor, and 8.00 GB of RAM. The molecular structures were first optimized before further calculations, including bond length and bond angle analysis. The Density Functional theory (DFT) method was employed, using the 6-31G basis set for non-metal atoms and the LANL2DZ basis set for ruthenium. These basis sets were implemented using the Gen keyword in Gaussian, along with the "Pseudo=Read" keyword. High Performance Computing (HPC) at UTM's Center for Information Communication and Technology (CICT) with Gaussian16 was also used to enhance computational efficiency.

The NLO properties were calculated after optimizing. The frequency-dependent first-order hyperpolarizability (β) was computed by using the "polar=gamma" keyword, combined with "CPHF=RdFreq" in the Gaussian job tab [10]. The calculations were performed at a laser frequency of 1064nm [11]. Data analysis and extraction were carried out upon completion of the calculations. The total first hyperpolarizability (β_{tot}) was determined using the following equation [12]:

$$\beta_{tot} = \left(\beta_x{}^2 + \beta_y{}^2 + \beta_z{}^2\right)^{0.5} \quad (1)$$

$$\beta_x = \beta_{xxx} + \beta_{xyy} + \beta_{xzz} \quad (2)$$

$$\beta_y = \beta_{yyy} + \beta_{yxx} + \beta_{yzz} \quad (3)$$

$$\beta_z = \beta_{zxx} + \beta_{zyy} + \beta_{zzz} \quad (4)$$

Results and Discussion

Experimental Studies

^{1}H NMR and ^{31}P NMR Spectroscopy Studies

All diaminophosphine ligands and complexes (Figure 1) were successfully synthesized, with percentage yields ranging from 36 to 69%.

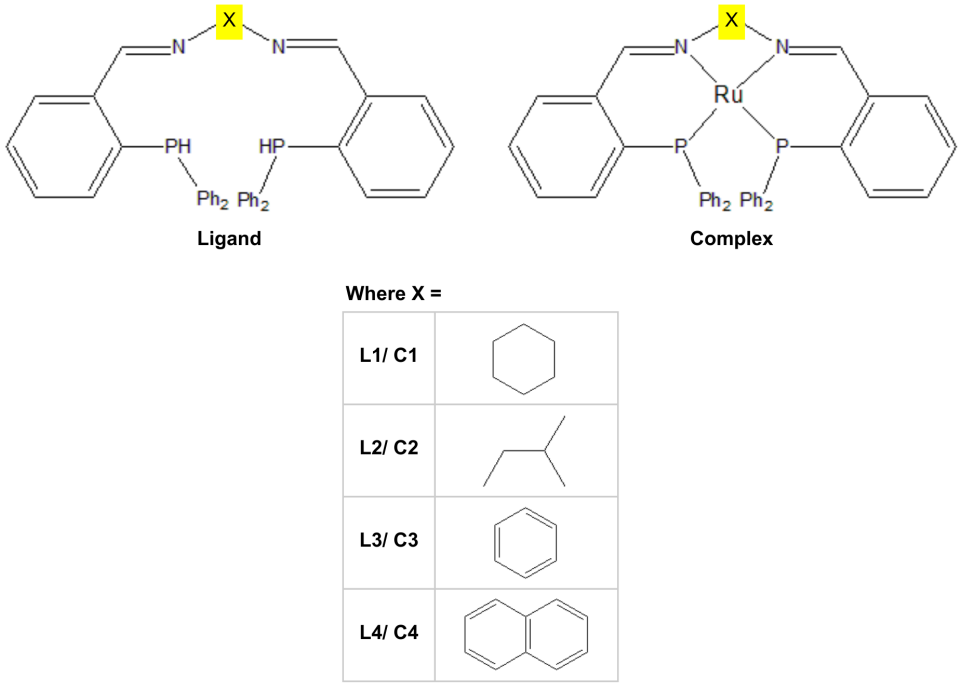

Figure 1. Structural representation of ligands (L1-L4) and complexes (C1-C4)

The studied compounds were analyzed using ^{1}H NMR and ^{31}P NMR spectroscopy in a deuterated chloroform solvent ($CDCl_3$) at 400 MHz to determine the number of protons and phosphorus atoms in the molecular structures. This data was also used to calculate magnetic properties that aid in predicting molecular geometry. Computational calculations were performed using the DFT/B3LYP/6-31G and DFT/B3LYP/GEN methods for optimized ligands and complexes. The GIAO method was applied for ^{1}H NMR, while no established reference exists for ^{31}P NMR in DFT studies. The chemical shifts were reported in ppm, relative to tetramethylsilane chemical shift (TMS) for ^{1}H NMR and ^{31}P NMR spectra. Computational calculations was conducted in the gas phase, whereas experimental values were obtained in solvent phase, which may account for differences between the two sets of data.

The ^{1}H NMR spectrum of L1 shown proton resonance signal at 8.67 ppm (s, 2H), corresponding to azomethine (-H-C=N) protons. The ^{1}H NMR spectrum of free ligands showed a multiplet for C-H aromatic protons in the range value of 6.76 - 7.73 ppm (28H, m, ArH). The main chemical shifts in this spectrum correspond to protons attached to the azomethine group (-H-C=N), which typically appear around δ 8 ppm in the downfield region due to the deshielding effect of the electronegative nitrogen atom. Other than that, aromatic protons usually appear between 6-8 ppm due to the conjugation effect in the benzene ring. The π-bonding electrons in the benzene ring act as conductors and hence, the protons become more deshielded and shifting the signals downfield [2]. For ^{31}P NMR, a peak at δ -13.73 ppm was observed, assigned to phosphorus in two equivalent phosphino ligands, which aligns well with literature values [8]. Similar findings were observed for L2-L4, as summarized in Table 1.

Table 1. Key ^{1}H and ^{31}P NMR data for synthesized ligands

Ligands	^{1}H NMR (CH=N), ppm	^{31}P NMR, ppm
L1	8.67	-13.73
L2	8.72	-13.11
L3	8.98	37.86
L4	8.15	32.17

For the complexes, ^{31}P NMR data confirmed the formation of desired the desired products. A downfield shift in the phosphorus peak from δ -13.73 ppm (L1) to δ 47.34 ppm (C1) was observed, indicating coordination of the phosphino ligand to the metal center. The strong singlet phosphorus peak suggests that the two phosphino groups in the ligand were coordinated and equivalent [13]. A similar trend was noted for C2-C4, as shown in Table 2.

Table 2. Key ^{1}H and ^{31}P NMR data for synthesized complexes

Complexes	^{1}H NMR (CH=N), ppm	^{31}P NMR, ppm
C1	8.93	47.34
C2	8.77	47.83
C3	8.98	50.28
C4	8.15	37.97

A comparison of experimental and computational ^{1}H NMR data for the ligand is summarized in Table 3. The percentage deviation between the experimental and computational data for the imine (-H-C=N) group was approximately 0.35%, while for aromatic protons (Ar-H), deviations ranged up to 4.82%. The deviation is likely due to solvent effects, as experimental data was obtained in $CDCl_3$, whereas computational calculations were conducted in gas phase.

Table 3. Summarized data of experimental and calculated ^{1}H NMR spectroscopy for ligands

Ligands		CH=N	C-H aromatic
L1	Experimental (ppm)	8.67	6.76-7.73
	Computational (ppm)	8.64	6.88-8.34
	% deviation	0.35	-
L2	Experimental (ppm)	8.71	6.79 - 7.89
	Computational (ppm)	8.29	7.12 - 7.94
	% deviation	4.82	-
L3	Experimental (ppm)	8.97	6.64-8.98
	Computational (ppm)	9.49	6.43-8.69
	% deviation	5.83	-
L4	Experimental (ppm)	8.15	6.04-8.05
	Computational (ppm)	8.62	6.90-8.01
	% deviation	8.62	-

The shift of the CH=N peak in L1 from δ 8.67 ppm to δ 8.93 ppm (C1) confirmed the coordination of ligand to the ruthenium metal (Table 4). Computational data predicted a CH=N peak at δ 9.09 ppm, giving a 1.82% deviation. In addition, the shift in aromatic proton peaks supports the presence of ruthenium metal and chlorine groups, which act as electron donating group. The chemical shift of aromatic proton of L1 at δ 6.76-7.73 ppm has shifted to δ 6.87-7.51 ppm for C1. Generally, deviations in computational and experimental data for the complexes ranges from 1.20% to 7.82%, indicating good agreement between the two applied methods.

Table 4. Summarized data of experimental and calculated ^{1}H NMR spectroscopy for complexes

Ligands		CH=N	C-H aromatic
C1	Experimental (ppm)	8.93	6.87-7.51
	Computational (ppm)	9.09	6.27-7.98
	% deviation	1.82	-
C2	Experimental (ppm)	8.77	6.59-7.63
	Computational (ppm)	8.66	6.34-8.39
	% deviation	1.20	-
C3	Experimental (ppm)	9.31	6.81-7.97
	Computational (ppm)	8.91	6.68-8.76
	% deviation	4.34	-
C4	Experimental (ppm)	8.20	7.12-7.69
	Computational (ppm)	8.84	6.13-7.81
	% deviation	7.82	-

Infrared Spectroscopy Studies

FTIR spectroscopy provides information on the stretching and bending frequencies of the functional groups based on bond vibrations. In this study, samples were prepared in KBr pellets by mixing the sample with solid KBr in a 1:3 ratio before analysis using FTIR spectroscopy. Computational data were obtained using the DFT/B3LYP/6-31G(d,p) and DFT/B3LYP/GEN methods for ligand and complexes respectively, with calculations performed in the gas phases. These methods are based on quantum chemistry principles, which can effectively account for electron movement within atom and are widely used for vibrational frequency calculations. By incorporating electron correlation to a certain extent, they provide more accurate results [7].

The main frequency observed in the Schiff base compound corresponds to the imine or azomethine (-HC=N) functional group, appearing in the range of 1640-1690 cm^{-1} [14]. The presence of this bond proves the formation of the Schiff base ligand through the reaction between an aldehyde and an amino group. A comparison between experimental and computational data is summarized in Table 5 and 6, along with the percentage deviation (%).

Table 5. Summary of FTIR spectroscopy data for ligands (L1-L4)

Ligands		C=N	CH=N	C-H aromatic	C=C aromatic
L1	Experimental (cm^{-1})	1638.08	3052.02	3257.02	1432.87
	Computational (cm^{-1})	1716.59	3037.86	3207.24	1475.82
	% deviation	4.79	0.46	1.53	3.00
L2	Experimental (cm^{-1})	1632.77	3052.48	3249.85	1432.73
	Computational (cm^{-1})	1728.52	3029.44	3203.01	1474.84
	% deviation	5.86	0.75	1.44	2.94
L3	Experimental (cm^{-1})	1693.42	3051.59	3306.11	1585.14
	Computational (cm^{-1})	1707.97	3064.50	3210.99	1603.98
	% deviation	0.86	0.42	2.88	1.20
L4	Experimental (cm^{-1})	1692.90	3053.44	3267.12	1481.57
	Computational (cm^{-1})	1709.75	3029.41	3199.18	1555.37
	% deviation	0.10	0.79	2.08	4.98

In the ligand spectra, the disappearance of the band at 3420 cm^{-1} attributed to the amino group, and the emergence of a new strong band at 1638.08 cm^{-1} for L1 assigned to the azomethine group ν(-C=N), confirm the formation of the Schiff base compound [15]. In L3, the C=C stretching vibration is observed at 1585 cm^{-1}, while the calculated spectrum shown a peak at 1604 cm^{-1}, with a percentage deviation of 1.20% [16]. The experimental C-H stretching band appears at 3306 cm^{-1}, whereas the computed value is 3211 cm^{-1}, resulting in a 2.88% deviation. The experimental C=N vibration is recorded at 1693 cm^{-1}, while the calculated value is 1708 cm^{-1}, with a deviation of 0.86%. For HC=N stretching, the experimental absorption occurs at 3052 cm^{-1}, while the computed value is 3065 cm^{-1}, with a deviation of 0.42%. A smaller percentage deviation indicates higher reliability of the data, as it reflects the accuracy of the basis set and computational method used for structure optimization.

The C=C stretching vibrations in the naphthyl ring normally occur between 1640 and 1400 cm^{-1}, and their corresponding wavenumbers indicate the degree of conjugation across the π-electron system [17]. For L4, the experimental spectrum exhibits strong absorption at 1693 cm^{-1} (C=N) and 3053 cm^{-1} (HC=N), confirming the formation of the ligand 2-(diphenylphosphino)benzaldehyde with naphthalene-1,8-diamine [15]. The corresponding calculated values are 1710 cm^{-1} (C=N) and 3029 cm^{-1} (HC=N), with percentage deviations of 0.10 % and 0.79% respectively. The presence of aromatic ring is confirmed by C-H aromatic stretching at 3267 cm^{-1} and C=C aromatic stretching at 1482 cm^{-1}. The computed values are 3199 cm^{-1} (C-H aromatic) and 1555 cm^{-1} (C=C aromatic), with percentage deviations of 2.08% and 4.98% respectively.

Table 6. Summary of FTIR spectroscopy data for complexes (C1-C4)

Complexes		C=N	CH=N	C-H aromatic	C=C aromatic
C1	Experimental (cm^{-1})	1625.86	3050.36	3213.00	1431.94
	Computational (cm^{-1})	1693.22	3076.45	3179.63	1476.95
	% deviation	4.14	0.85	1.04	3.14
C2	Experimental (cm^{-1})	1628.71	3051.27	3140.37	1432.19
	Computational (cm^{-1})	1707.12	3082.42	3202.53	1461.50
	% deviation	4.81	1.02	1.98	2.04
C3	Experimental (cm^{-1})	1619.19	2923.48	3054.96	1587.93
	Computational (cm^{-1})	1695.82	3123.37	3201.99	1608.43
	% deviation	4.73	6.84	4.81	1.32
C4	Experimental (cm^{-1})	1590.15	3053.87	3293.87	1436.35
	Computational (cm^{-1})	1594.28	3121.20	3206.66	1469.47
	% deviation	0.26	2.20	2.65	2.31

All complexes (C1-C4) show characteristic bands that confirm coordination of the Schiff base ligands to the metal center. Notably, all complexes exhibit strong absorption bands corresponding to the azomethine (C=N) and imine (CH=N) groups, which are useful indicators for metal-ligand interaction [8]. The C=N stretching bands appear in the range of 1590-1629 cm^{-1},which are slightly red-shifted compared to the free ligands (1633-1693 cm^{-1}). This shift suggests coordination through the azomethine nitrogen, weakening the C=N bond due to electron delocalization with the metal center [18]. For instance, L1 shows a C=N stretch at 1683 cm^{-1}, shifting to 1626 cm^{-1} in C1. Similarly, L4 shows a shift from 1693 cm^{-1} to 1590 cm^{-1} in C4. The computed C=N frequencies support this trend, with percentage deviations mostly below 5%.

CH=N bands also show minor shifts upon complexation, generally remaining within 3050-3054 cm^{-1} across the complexes, compared to 3051-3053 cm^{-1} in the ligands. These subtle changes reflect the electronic effect of coordination without significant structural distortion [19]. For example, L2 and C2 both show CH=N absorption at ~3051 cm^{-1} with only ~1% deviation from calculated values. However, C3 exhibits a relatively higher deviation (6.84%) between the experimental and computational CH=N stretching frequencies. This can be attributed to the rigid phenyl backbone which restricts bond flexibility and alters electron delocalization, leading to discrepancies between experimental and theoretical values [20]. Aromatic C-H and C=C stretches are retained in the spectra, though slight shifts in position and intensity changes further support ligand coordination. The spectral patterns and low percentage deviations between experimental and theoretical values (<7%) confirm that DFT methods provide a good approximation of vibrational behaviour in both ligands and their complexes.

Ultraviolet-Visible Spectroscopy Studies

UV-Vis spectroscopy provides insights into MLCT and LMCT interactions between the ruthenium metal center and phosphine ligands. The experimental measurements were recorded in the wavelength range of 200-800 nm, with ligand and complex concentrations set $1x10^{-4}$ M and $1x10^{-6}$ M respectively. Theoretical spectra were obtained via TD-DFT/B3LYP/6-31G(d,p) calculations in the gas phase.

All ligands (L1-L4) showed theoretical π-π* and n-π* transitions between 290-370 nm. Notably, L1 and L2 showed similar calculated peaks at ~295 and ~370 nm, attributed to n-π* and π-π* transitions, but no experimental spectra were recorded, likely due to instability in solution [21]. L3 exhibited a strong experimental π-π* band at 398.5 nm, closely matching the calculated 386.6 nm (2.99% deviation), validating the TD-DFT method. L4 showed a red-shifted π-π* band at 567.5 nm, indicating stronger intramolecular charge transfer effects [22]. UV-Vis data for L1-L4 is summarized in Table 7.

Table 7. Summary of UV-Vis spectroscopy data for ligands (L1-L4)

Ligands	λ_{max} (Experimental, nm)	λ_{max} (Theoretical, nm)	Transition type
L1	-	297.57, 370.27	n-π*, π-π*
L2	-	293.50, 365.90	n-π*, π-π*
L3	398.50	386.57	π-π*, P-P*
L4	567.50	447.00	π-π*, P-P*

Complexation with Ru(II) caused red shift and increased intensities, which are the characteristics of MLCT transitions [23]. While C1 and C2 could not be measured experimentally due to solvent effects, TD-DFT predicted MLCT absorptions at 495.7 and 510.8 nm respectively. C3 showed significantly increase in molar absorptivity (ε=23500 $M^{-1}cm^{-1}$) compared to L3 (ε=9800 $M^{-1}cm^{-1}$), confirming stronger conjugation and charge transfer upon coordination. Its spectrum featured MLCT and d-d transitions at 422.0 and 542.5 nm respectively [24]. C4 exhibited transitions with the longest wavelength among all compounds at 564.5 nm (MLCT) and 718.5 nm (d-d), but with an intensity lower than C3, suggesting reduced charge transfer efficiency [22]. The UV-Vis data for C1-C4 is summarized in Table 8.

Table 8. Summary of UV-Vis spectroscopy data for complexes (C1-C4)

Ligands	λ_{max} (Experimental, nm)	λ_{max} (Theoretical, nm)	Transition type
C1	-	495.74	MLCT
C2	-	510.79	MLCT
C3	542.50, 422.00	1010.12	d-d, MLCT
C4	718.50, 564.50	686.74	d-d, MLCT

Theoretical Studies

Geometry Optimization

Geometry optimization is the process of determining the stationary points on the potential energy surface by calculating the molecular geometry and energy. It provides insights into the structure's energy, the geometry at the lowest possible energy state, bond angles and bond lengths [7]. A lower energy value indicates a more stable compound. The calculation iterates until the lowest ground-state energy is achieved, signifying convergence, which means the optimization cycle is complete. The geometry optimization of all studied compounds (L1-L4 and C1-C4) was performed using the DFT/B3LYP/6-31G(d,p) and GEN level of theory without any symmetrical constraints. These calculations were executed using Gaussian software under zero charge and single spin multiplicity to obtain molecular energy, bond lengths, bond angles and dipole. The DFT method describes the electron density within a molecule based on quantum chemistry principle [25]. The percentage deviation for all bond angles computed using the DFT approach ranged from 0.53% to 4.39%, calculated using Equation 1. DFT calculations explicitly consider the electron correlation effect, which improves accuracy. A deviation below 5% is considered low, indicating adequate accuracy.

$$Percentage\ deviation = \frac{Calculated\ value - Experimental\ value}{Experimental\ value} \times 100\% \quad (5)$$

All studied compounds revealed that the ruthenium complexes exhibit lower molecular energy compared to the free ligands, confirming that metal-ligand coordination enhances structural stability [15]. Among the ligands, L4 showed the lowest molecular energy (-2643.03 a.u.), followed by L1 (-2493.01 a.u.), L3 (-2489.46 a.u.), and L2 (-2376.27 a.u.). The enhanced stability of L4 may be attributed to the rigid, planar naphthalene backbone which facilitates stronger conjugation, leading to a more effective intramolecular charge delocalization [26]. In contrast, L2 having a more flexible propane core exhibited the highest energy, possibly due to less favourable orbital overlap. These trends emphasize the influence of diamine backbone rigidity and aromacity on ligand stability [27]. On the other hand, C4 showed the highest molecular energy (-3657.40 a.u.) among the complexes, followed by C3 (-3503.77 a.u.), C1 (-3507.43 a.u.), and C2 (-3390.70 a.u.). This trend mirrors the stability observed in their corresponding ligands, further supporting the correlation between ligand structure and complex stability. The molecular energy of the studied compounds is summarized in Table 9.

Table 9. Molecular energies of ligands (L1-L4) and complexes (C1-C4) calculated using DFT

Compound	Molecular energy (a.u.)
L1	-2493.01
L2	-2376.27
L3	-2489.46
L4	-2643.03
C1	-3507.43
C2	-3390.70
C3	-3503.77
C4	-3657.40

The selected bond lengths and bond angles for ligands and ruthenium complexes are summarized in Table 10 and 11 respectively. In the ligands, typical C=N and C-N bond lengths were observed, with slight variations across L1 to L4 [28]. For instance, the C=N bond length ranged from 1.272 Å (C2) to 1.300 Å (C4), aligning well with known imine linkage values. Upon coordination, notable changes were observed. The Ru-N and Ru-P bond lengths varies slightly among complexes. For example, Ru-N distances ranged from 2.116 Å (C3) to 2.229 Å (C4), while Ru-P distances were shortest in C3 (2.292 Å), supporting stronger metal-ligand interactions in this complex.

The bond angle analysis shows that all complexes adopt distorted octahedral geometries around the ruthenium centre. The Cl-Ru-Cl angles in all complexes are close to linear, ranging from 172.35° (C3) to 174.66° (C4), with percentage deviations between 0.53% and 1.87% from ideal geometries [28]. Complexes C1 and C2 also exhibit typical octahedral features, with N_1-Ru-P_1 angles of 87.99° and 87.47° respectively, and N_1-Ru-N_2 angles around 81°. Interestingly, C3 and C4 show more significant angular distortions, such as the compressed N_1-Ru-P_2 angle in C3 (166.06°) and the expanded N_1-Ru-P_2 angle in C4 (168.91°), likely due to increased steric strain or ligand flexibility [21]. Moreover, the P-Ru-P and N-Ru-N angles indicate that phosphorus and nitrogen atoms adopt a cis-position, particularly evident in complexes C3 and C4. These deviations from ideal geometry are indicative of chelation effects and ring strain, especially in metalacyclic structures [16]. Overall, the DFT-optimized structures are consistent with experimental values and literature data, validating the reliability of B3LYP and GEN methods used. These optimized structures were further employed in FTIR, NMR, and UV-vis spectroscopy analyses. The atom labelling scheme for the ligands and complexes is presented in Table 12.

Table 10. Selected bond length (Å) for ligands and ruthenium complexes

Atomic Bond	Bond Length (Å)								
	L1	**C1**	**L2**	**C2**	**L3**	**C3**	**L4**	**C4**	**Previous work [28]**
C_1-N_1	1.464	1.444	1.452	1.454	1.408	1.437	1.401	1.421	1.504
C_2=N_1	1.274	1.269	1.275	1.272	1.283	1.296	1.277	1.300	1.290
Ru-N_1	-	2.118	-	2.136	-	2.116	-	2.229	2.183
Ru-P_1	-	2.381	-	2.374	-	2.292	-	2.387	2.2957
Ru-Cl_1	-	2.513	-	2.498	-	2.494	-	2.487	2.4164

Table 11. Selected bond angle (°) for ruthenium complexes

Bond	Bond Angle (°)				
	C1	**C2**	**C3**	**C4**	**Previous work [28]**
N_1-Ru-P_1	87.99	87.47	82.84	80.17	81.30
N_1-Ru-P_2	133.51	121.70	166.06	168.91	172.54
P_1-Ru-P_2	100.02	104.23	107.50	102.89	106.10
N_1-Ru-Cl_1	84.90	84.67	93.49	94.06	90.09
N_1-Ru-N_2	80.88	81.19	87.46	88.59	91.30
P_1-Ru-Cl_1	93.53	94.91	97.12	93.12	94.23
P_1-Ru-Cl_2	88.17	92.81	89.51	85.68	88.43
Cl_1-Ru-Cl_2	172.61	172.44	172.35	174.66	175.58

Table 12. Atom labelling scheme of ligands (L1-L4) and complexes (C1-C4)

Compound	Structure
L1	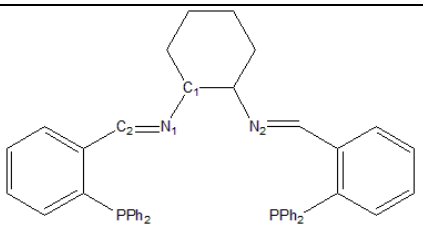
L2	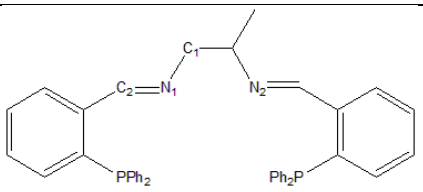
L3	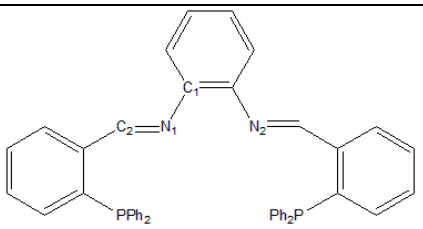
L4	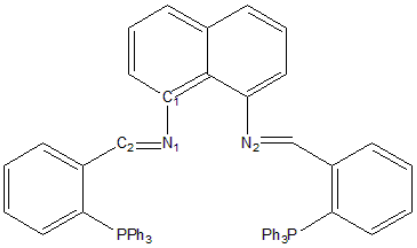
C1	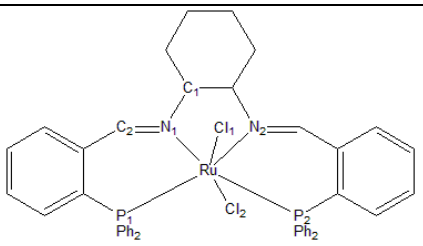
C2	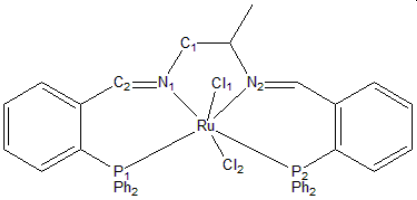

C3	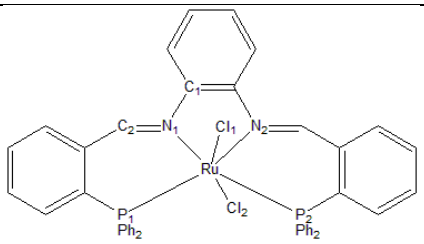
C4	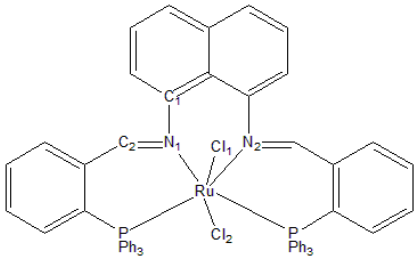

Molecular Electrostatic Potential Plot

The MEP plot depicts the positive, negative, and neutral electrostatic potential regions of a molecular surface using distinct colours. It is a valuable tool for identifying nucleophilic and electrophilic attack sites, as well as hydrogen-bonding interactions [29]. The molecular electrostatic potential minima, corresponding to regions of negative charge density help predict electrophilic reaction sites. The topographical distribution reveals subtle variations in the three-dimensional electronic structure.

Figure 3 shows the MEP maps of the studied compounds, computed using the B3LYP method with the 6-31G(d,p) basis set. The red regions indicate electron-rich areas favourable for electrophilic attack, whereas the blue regions represent electron-deficient sites suitable for nucleophilic attack [18]. The green regions denote neutral charge distributions.

In C3 and C4, the absence of red regions suggests strong metal-ligand coordination, consistent with the presence of rigid and π-conjugated diamine linkers (phenyl-based linker in L3 and naphthalene-based linker in L4) [15]. These structures likely promote better orbital overlap and delocalization upon complexation, resulting in reduced localized electron density near the donor atoms. In contrast, L1 and L2 with more flexible aliphatic cyclohexane and propane linkers, retain more pronounced red regions near nitrogen and phosphorus atoms, especially in their uncoordinated states, suggesting weaker delocalization and greater nucleophilicity [30]. Upon complexation (C1 and C2), these red regions diminish but are still more localized compared to C3 and C4, indicating comparatively weaker metal-ligand interactions [7].

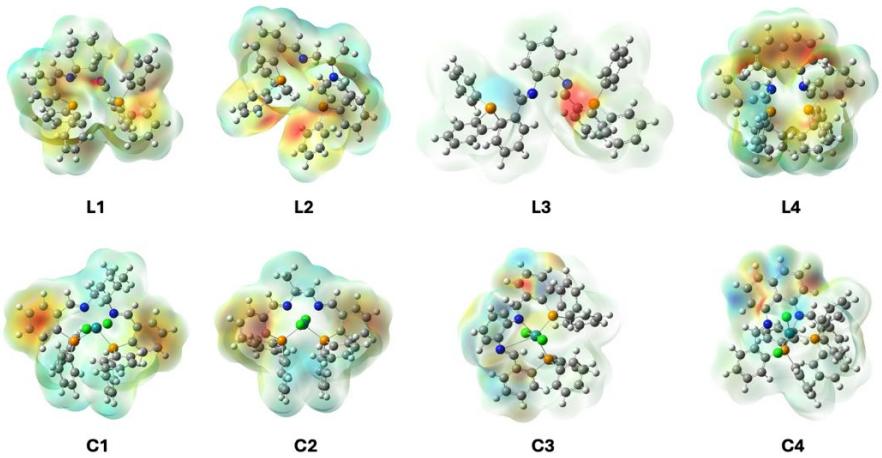

Figure 2. 3D MEP maps of ligands (L1-L4) and complexes (C1-C4)

Nonlinear Optical Studies

Phosphine ligands in organometallic complexes follow the general formula of PR_3, where the R group in this study is a phenyl group. These phosphine ligands act as electron acceptors, allowing the complexes to exhibit NLO properties [31]. The presence of this ligand facilitates electron back-donation from the ruthenium metal to the ligand (π-back bonding), leading to MLCT. This interaction enhances the stability of the complexes, making them promising NLO candidates. Ruthenium serves as a donor due to its electron rich *d*-orbital (d^6) configuration, which allows effective electron donation and polarizability, key factors for NLO activity [32]. The phenyl group acts as a *σ*-bond donor, which interacts with phosphorus atom's lone pair to form *σ*-bond. This bonding contributes to enhanced NLO properties, alongside electron back-donation from the metal's *d*-orbital to the vacant orbitals of phosphorus. All the electron transfer will enhance the stability of the complexes [33]. Bonding between ruthenium with nitrogen should also be highlighted in this discussion. The nitrogen atom in these complexes acts as an electron donor, forming a σ-bond with the metal, while the nonbonding t_{2g} orbital of ruthenium donates electrons to the nitrogen's vacant π* orbitals, creating π-back bonding. Similar bonding behaviour has been observed in other transition metal-ligand systems, where such π-back donation stabilizes charge-separated states, thereby enhancing NLO properties [34, 35].

When ruthenium is coordinated with ligands containing different electron-donating or withdrawing groups, as well as varying conjugated systems, the electronic structure and charge transfer characteristics are altered, leading to variations in NLO properties [16]. The dipole moment and the HOMO-LUMO energy gap can be used to determine the first-order hyperpolarizability (β_{tot}), an indicator of second-order NLO characteristics [36]. The dipole moments of the studied compounds are summarized in Table 13. The results indicate that a higher dipole moment correlates with greater NLO activity due to enhanced charge redistribution and electron transfer. Khairul, *et al*. [37] also stated that dipole moments in a compound arise from charge separation and differences in electronegativity. Thus, compounds with the higher dipole moments exhibit greater electron density redistribution and increased charge transfer.

Table 13. Dipole moment of studied compounds.

Compound	Dipole Moment (Debye)
L1	1.73
L2	1.90
L3	2.84
L4	1.34
C1	0.24
C2	0.18
C3	3.50
C4	9.67

The total frequency-dependent first hyperpolarizability (β_{tot}) values are summarized in Table 14 and 15. These values were derived from the β (-2ω, ω, ω) based on the second-harmonic generation (SHG) calculations at a wavelength of 1064 nm. β_{tot} is a key parameter representing second-order hyperpolarizability, which directly correlates with NLO properties [38]. The vector value of β was used to calculate the β_{tot} as shown in the 'Computational Method' section. The β_{tot} value of L1 (28.287×10^{-30} esu) is higher than that of L2 (24.599×10^{-30} esu) due to the stabilizing effect of its cyclohexane ring, which provides structural rigidity compared to L2, which only contains a methyl group. In contrast to L1 and L2, L3 and L4 showed enhanced NLO properties, with β_{tot} values of 141.13×10^{-30} esu and 185.23×10^{-30} esu respectively. This increase is due to their extended π-conjugation and presence of polarizable substituents, which facilitate intramolecular charge transfer [22]. Interestingly, L4 showed the highest β_{tot} among all ligands, supported by a significant dipole moment (1.34 D), suggesting effective electron delocalization and polarizability within the molecular structure. A similar trend was observed in a study on Cu(II) Schiff base complexes with ferrocenyl donors, where β values increased with stronger electron-withdrawing groups (Cl < Br < F < NO_2), attributed to enhanced donor-acceptor interactions and conjugation within the complex framework [30].

Upon complexation with ruthenium, C1 and C2 also exhibit NLO properties, though their values are lower due to the presence of linear and cyclic alkane substituents, which lack extensive electron delocalization [24]. However, C1 shows the highest β_{tot} value (781.277×10^{-30} esu), followed by C2 (206.622×10^{-30} esu). This aligns with the principle that higher dipole moments correspond to greater β_{tot} values due to increased electron density redistribution and greater charge transfer [33]. C1 shows higher dipole

moment than C2 and thus, it is proven that C1 is a better NLO candidate compared to C2. It can be concluded that higher dipole moment leads to a higher β_{tot} value. Moreover, the cyclic substituent in C1 enhances rigidity and stability, whereas the methyl group in C2 acts as a weak electron donor, contributing to the electron transfer and dipole moment, albeit to a lesser extent than conjugated systems. The β_{tot} value of L1 increases by 28 times upon coordination with ruthenium to form C1, while the increase for L2 to C2 is eightfold. This demonstrates that incorporating ruthenium significantly enhances NLO properties due to MLCT and LMCT.

On the other hand, C3 and C4 exhibited a substantial increase in hyperpolarizability, with β_{tot} values of 6748.34 x 10^{-30} esu and 1213.06 x 10^{-30} esu respectively. Notably, C3 showed the highest β_{tot} value among all studied complexes, consistent with its large dipole moment (3.50 D). This implies extensive MLCT and strong donor-acceptor interaction within the conjugation system [2]. Although C4 has the highest dipole moment (9.67 D), it exhibits a lower β_{tot} than C3, indicating that dipole moment alone does not fully determine NLO activity, the extent of conjugation and charge delocalization also play critical roles. This trend is consistent with the findings of prior studies on conjugated organic dyes such as hexylcarbazole (HC), 4,7-bis(thiophen-2-yl)benzo[c][1,2,5]thiadiazole (DTBT), and their extended D-A-D conjugated polymer PCTB. In that work, increased conjugation from HC to DTBT to PCTB led to systematically enhanced NLO responses as observed via Z-scan experiments [39].

Table 14. β_{tot} values of ligands (L1-L4)

β_{tot} (x10^{-30} esu)	Ligands			
	L1	L2	L3	L4
β_{xxx}	-6.13	1.24	10.44	0.005
β_{xyy}	-1.82	0.45	0.45	0.001
β_{xzz}	0.26	-0.74	-17.18	0.01
β_{yyy}	-1.20	0.11	0.94	0.001
β_{yxx}	-2.79	0.75	8.51	-0.001
β_{yzz}	2.17	-0.68	8.61	0.005
β_{zxx}	0.88	4.24	4.51	10.30
β_{zyy}	3.19	1.80	3.85	5.40
β_{zzz}	1.56	2.28	31.16	50.62
β_{x}	-22.30	2.79	-13.72	0.0467
β_{y}	-4.76	0.54	63.97	0.0165
β_{z}	16.90	24.43	126.54	185.28
β_{tot}	28.38	24.59	141.13	185.23

Table 15. β_{tot} values of complexes (L1-L4)

β_{tot} (x10^{-30} esu)	Ligands			
	C1	C2	C3	C4
β_{xxx}	-6.27	-2.43	-174.79	4.29
β_{xyy}	-8.98	2.12	-365.31	10.55
β_{xzz}	-9.63	-32.34	987.21	11.35
β_{yyy}	-12.77	0.93	591.86	-341.20
β_{yxx}	-9.11	-16.96	-43.77	-167.71
β_{yzz}	-9.25	-3.80	812.33	-64.02
β_{zxx}	-21.57	20.58	292.95	-2.22
β_{zyy}	-57.11	-0.54	657.72	17.08
β_{zzz}	-208.19	13.71	1237.68	-34.74
β_{x}	-118.98	-71.58	-356.44	98.004
β_{y}	-178.03	-129.01	4871.53	-1208.45
β_{z}	-751.35	144.64	4656.31	-39.512
β_{tot}	781.27	206.62	6748.34	1213.06

Frontier Molecular Orbital Theory

HOMO and LUMO energy levels play a crucial role in predicting NLO behaviour. The HOMO represents the electron-rich donor site, while the LUMO serves as the most likely electron-accepting site. The

HOMO-LUMO energy gap (E_{gap}) is inversely proportional to NLO properties, as a smaller gap facilitates greater charge transfer within the electron delocalization system, enhancing NLO activity [38]. The E_{gap} is calculated using the following formula:

$$E_{gap} = E_{LUMO} - E_{HOMO} \quad (6)$$

The data in Table 16 reveal that L4 has the lowest energy gap (0.42 eV) among the ligands, while C3 exhibits the lowest value (0.37 eV) among the complexes. A general trend of reduced band gaps upon complexation with ruthenium is observed, supporting the hypothesis that conjugation and charge transfer play significant roles in modulating NLO properties [26]. Notably, the conjugation in the benzene ring of L3 decreases the band gap from L1 (2.01 eV) by 1.28 eV. Similarly, complexation reduced the band gap from C1 (0.70 eV) to C3 (0.37 eV) complexes, highlighting the importance of conjugation.

Table 16. HOMO, LUMO energy and band gap of the studied compounds

Compound	HOMO (eV)	LUMO (eV)	Band Gap
L1	-8.01	-5.99	2.01
L2	-8.06	-5.94	2.12
L3	-8.11	-6.37	1.74
L4	-5.77	-6.19	0.42
C1	-6.22	-5.52	0.70
C2	-6.19	-5.52	0.66
C3	-6.25	-5.88	0.37
C4	-6.19	-5.77	0.42

Figure 4 and 5 show the comparison of HOMO-LUMO energy gaps between ligands and their corresponding complexes. The diagram clearly illustrates the energy gap between the HOMO and LUMO. The green regions in the molecular structures indicate areas of low electron density, whereas the red regions signify areas of high electron density. From the diagram, it is evident that ligands exhibit wider band gap compared to the complexes. This reduction in the band gap upon complex formation is attributed to π-back bonding from the metal to the ligand, which introduces a push-pull electronic system [40]. This phenomenon significantly influences the electronic properties of the complexes, thereby affecting their NLO properties. Additionally, frontier molecular orbital analysis reveals that the charge transfer occurs in the complexes occurs due to electron-donating effect of the amine derivatives, which push electron density toward the ruthenium center [41]. This is reflected in the HOMO, where electron density is concentrated around the donor region, while in the LUMO, the electron density shifts towards the acceptor region. Specifically, a higher electron density at the amine derivates is observed in the HOMO, whereas in the LUMO, electron density is more prominent around the Cl-Ru fragment.

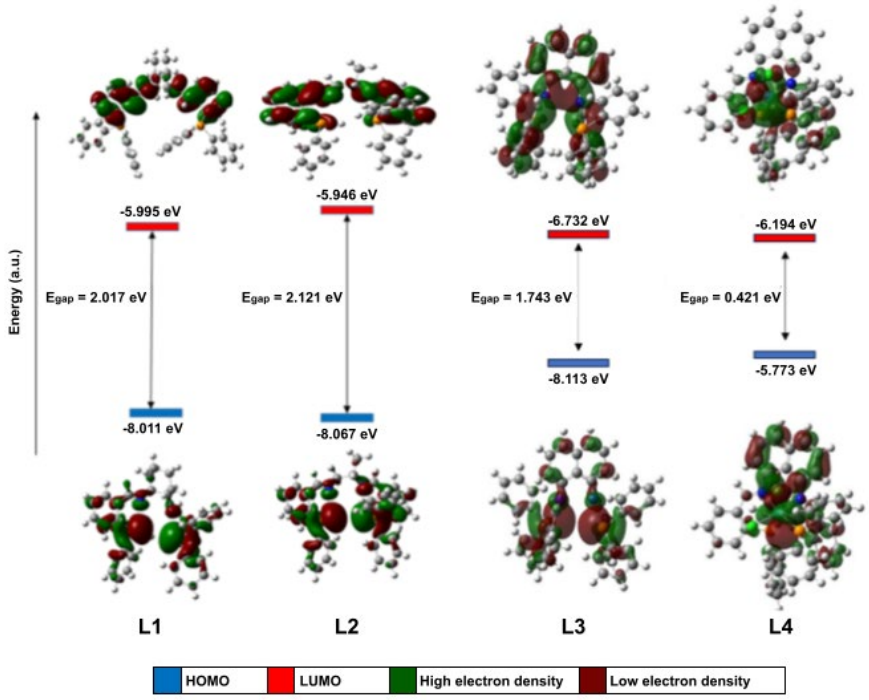

Figure 3. Frontier molecular orbitals for ligands (L1-L4)

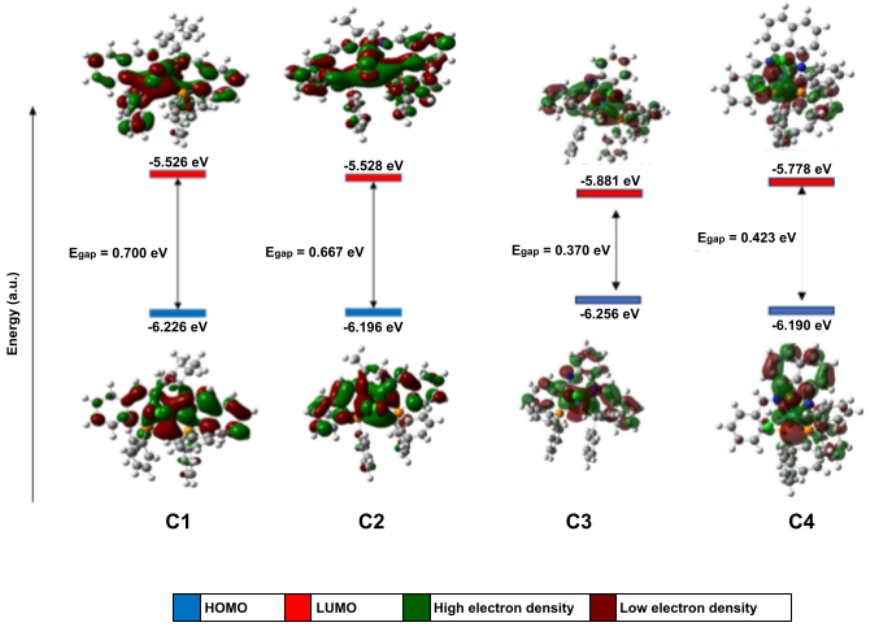

Figure 4. Frontier molecular orbitals for complexes (C1-C4)

Structure to NLO Properties

The relationship between dipole moment and band gap in the context of NLO materials is an intriguing area of research. However, this relationship is not always straightforward, as it depends on factors such as molecular structure and experimental conditions. While both dipole moment and band gap are significant properties in NLO studies, their correlation is often influenced by additional factors. Dipole moment measures the separation between positive and negative charges in a molecule, reflecting its

overall polarity or charge distribution asymmetry. In NLO materials, a non-zero dipole moment is generally desirable, as it enhances NLO effects.

An analysis of the data in Table 17 compares the band gap, dipole moment, and the first-order hyperpolarizability (β_{tot}) of the ligands (L1-L4) and complexes (C1-C4). The findings indicate that the complexes exhibit significantly higher NLO responses (higher β_{tot} values) than the ligands. Upon complexation, NLO increases dramatically, with percentage increments ranging from approximately 555% to 4667%. Moreover, the complexes also show lower band gaps than the ligands, suggesting that metal complexation enhances NLO activity while simultaneously reducing the band gap (Figure 5). This enhancement is consistent with theoretical findings in previous studies, where large β_{tot} was due to strong intramolecular charge transfer between the transition metal and the coordinated ligands [34].

No significant correlation between dipole moment and NLO response was observed in this study. To better understand the intricate relationships among dipole moment, band gap, and NLO properties, further investigations are necessary. Future research should explore a wider range of materials and experimental conditions to clarify the specific role of dipole moment in NLO behaviour. Such studies will contribute to the advancement of NLO and the design of materials with optimized NLO properties.

Table 17. Comparison of band gap, dipole moment, and β_{tot} value for ligands (L1-L4) and complexes (C1-C4)

Compound	Band Gap (eV)	Dipole moment (Debye)	β_{tot} (x10^{-30} esu)
L1	2.0170	1.73	28.237
L2	2.1210	1.90	24.599
L3	0.7325	2.85	141.130
L4	1.7402	1.35	185.230
C1	0.7000	0.24	781.277
C2	0.6670	0.18	206.622
C3	0.3750	3.51	6748.340
C4	0.4204	9.67	1213.060

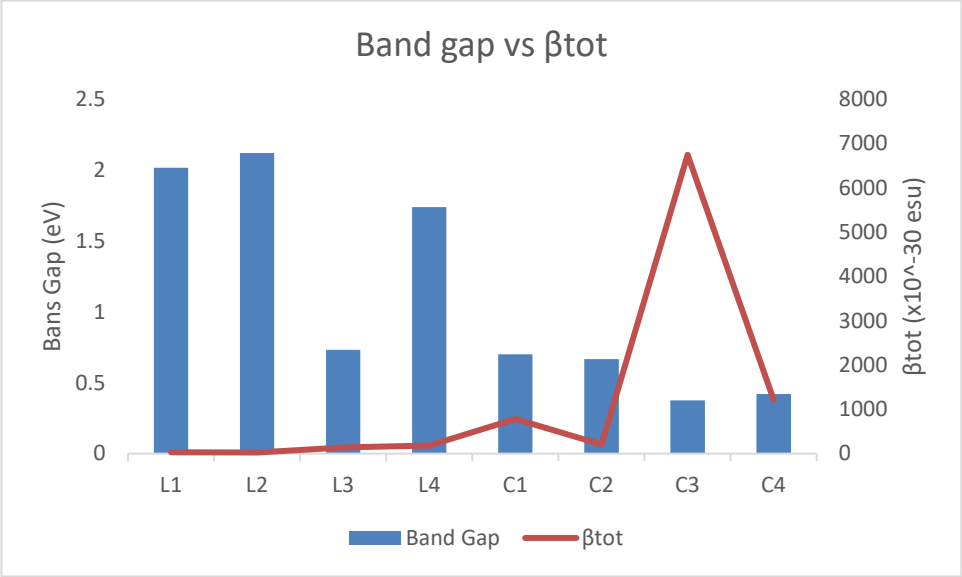

Figure 5. Comparison of band gap versus β_{tot}

Conclusions

A total of eight compounds were successfully synthesized and characterized using FTIR, UV-Vis, and NMR spectroscopy. The interactions between the ligands and the Ruthenium metal were confirmed through spectral shifts in FTIR and UV-Vis analysis. Computational studies using DFT method revealed the impact of different π-conjugated substituents on the electronic and NLO properties of the

compounds. The results showed that ruthenium complexes exhibited significantly higher NLO responses than their corresponding ligands. Recommendations for future research include exploring the effects of different substituents and metal centers for improved NLO activity, investigating additional π-conjugated substituents to enhance the NLO response, and exploring the applications of machine learning techniques, such as data mining, neural networks, or genetic algorithms, to analyze and predict NLO properties based on DFT data. This could accelerate the development of predictive models and the discovery of new compounds with desired NLO properties. This research provides valuable insights into the design and development of materials with enhanced NLO characteristics, contributing to advancements in NLO and materials science.

Conflicts of Interest

The authors declares that there is no conflict of interest regarding the publication of this paper.

Acknowledgment

This research was funded by MINISTRY OF HIGHER EDUCATION, MALAYSIA, grant number FRGS/1/2021/STG04/UTM/02/7 and UNIVERSITI TEKNOLOGI MALAYSIA, UTM CG, PY/2024/02436/ Q.J130000.3054.05M08.

References

[1] Soliman, A. M., El-Remaily, M. A. E. A. A. A., Kamel, M. S., El-Araby, A., & Shokr, E. K. (2025). Synthesis, optical linear and non-linear characterization and metal ion sensing application of some novel thieno[2,3-b]thiophene-2,5-dicarbohydrazide Schiff base derivatives. *Scientific Reports, 15*(1), 1611. https://doi.org/10.1038/s41598-025-1611.

[2] Sharma, V., Chandra, R., Dutta, S., Sahu, D., & Patra, G. K. (2024). Schiff base and organic ligand stabilized metal nanoparticles as potential chemosensors for hazardous metal ions: Design, principle, optical signaling mechanism and application. *Inorganica Chimica Acta*, 122321. https://doi.org/10.1016/j.ica.2023.122321.

[3] Petrovskaia, A., *et al.* (2024). Dual emissive mono- and bis-alkynylpyridinium Pt(II) complexes: Synthesis and luminescent properties. *Organometallics, 43*(20), 2495–2504. https://doi.org/10.1021/acs.organomet.4c00295.

[4] St. Onge, P. B. (2023). Dynamic metal-ligand interactions in semiconducting π-conjugated materials/ Doctoral dissertation. University of Windsor).

[5] Santos, F. A., Cardoso, C. E., Rodrigues, J. J., Jr., De Boni, L., & Abegão, L. M. (2023). Nonlinear optical materials: Predicting the first-order molecular hyperpolarizability of organic molecular structures. *Photonics, 10*(5), 545. https://doi.org/10.3390/photonics10050545.

[6] Zhao, Y., Xiong, M., Wang, D., Xu, B., & Baesso, M. L. (2024). First single-frequency Pr:LiYF4 ring laser at green. *Optics & Laser Technology, 168*, 109960. https://doi.org/10.1016/j.optlastec.2023.109960.

[7] Arunkumar, A., & Ju, X. H. (2024). Computational method on highly efficient D-π-A-π-D-based different molecular acceptors for organic solar cells applications and non-linear optical behaviour. *Spectrochimica Acta Part A: Molecular and Biomolecular Spectroscopy, 317*, 124391. https://doi.org/10.1016/j.saa.2023.124391.

[8] Pang, S., Jillani, M., & Razak, F. I. A. (2023). Synthesis, characterization and density functional theory (DFT) study on the zinc metal complex for nonlinear optical application. *Journal of Materials in Life Sciences (JOMALISC)*, 141–146.

[9] Ronchi, E. (2022). Development and study of novel catalytic reactions to efficiently address synthetic challenges: Enantioselective multicomponent synthesis of homoallylic amines and site-selective debenzylation of mono- and disaccharides. Doctoral dissertation. Harvard University.

[10] Zhou, S., Sun, M., & Zheng, Y. (2024). Physical insight into optical spectroscopy of chiral covalent organic pillars as molecular nanotubes. *Physica E: Low-dimensional Systems and Nanostructures, 159*, 115926. https://doi.org/10.1016/j.physe.2023.115926.

[11] Nadeem, S., Anwar, A., Khan, M. U., Hassan, A. U., & Alrashidi, K. A. (2024). Exploring the ON/OFF nonlinear optical (NLO) response in tetracene-based chromophores: A DFT study on solvent and frequency-dependent NLO properties for switching applications. *Journal of Molecular Liquids, 411*, 125730. https://doi.org/10.1016/j.molliq.2023.125730.

[12] Khemalapure, S. S., *et al*. (2020). Structural, spectroscopic and computational investigations on (4,6-dimethylbenzofuran-3-yl)-acetic acid hydrazide. *Journal of Molecular Structure*. Advance online publication. https://doi.org/10.1016/j.molstruc.2020.128748.

[13] Le, L. H., Pham, N. H., Tran, P. D., & To, T. H. (2025). Synthesis of an imine-type nickel complex and investigation of its electrocatalytic activity for H2 evolution. *RSC Advances, 15*(4), 2430–2436. https://doi.org/10.1039/D4RA08023J.

[14] Avcı, D., Özge, Ö., Sönmez, F., Başoğlu, A., Tamer, Ö., & Atalay, Y. (2024). Novel Schiff base-azide metal complexes: Synthesis, spectral, nonlinear optics, and DFT studies. *Materials Science in Semiconductor Processing, 179*, 108523. https://doi.org/10.1016/j.mssp.2023.108523.

[15] Arabahmadi, R., Kamali, S., & Sharafi, A. R. (2025). Two new cobalt(II) and copper(II) complexes with azo-azomethine ligand: Synthesis, antioxidant and antibacterial activities, thermal investigations, DFT calculations,

and molecular docking studies. *Journal of Molecular Structure, 1337*, 142177. https://doi.org/10.1016/j.molstruc.2025.142177.
[16] Muslim, M., *et al.* (2025). Exploring superior nonlinear optical properties of copper complexes with π-conjugated ligands: Experimental and theoretical investigation. *RSC Advances, 15*(6), 4657–4668. https://doi.org/10.1039/D4RA07693C.
[17] Lv, J., *et al*. (2022). Schiff base-type Cu(I) complexes containing naphthylpyridyl-methanimine ligands featuring higher light-absorption capability: Synthesis, structures, and photophysical properties. *Polyhedron, 224*, 116002. https://doi.org/10.1016/j.poly.2022.116002.
[18] Jillani, M., Athirah, N., Sapari, S., & Razak, F. I. A. (2023). Investigating the effect of tuning the metal center in complexes for nonlinear optical application. *Malaysian Journal of Fundamental and Applied Sciences, 19*(5), 817–826. https://doi.org/10.11113/mjfas.v19n5.4104.
[19] Wu, Z. P., *et al.* (2021). Manipulating the local coordination and electronic structures for efficient electrocatalytic oxygen evolution. *Advanced Materials, 33*(40), 2103004. https://doi.org/10.1002/adma.202103004.
[20] Abdou, A. (2025). Synthesis, structural, DFT, in vitro biological exploration, and DNA interaction of new Ni(II) and Cu(II) mixed-ligand complexes featuring 2,2′-pyridine-2,6-diylbis(1H-benzimidazole) and 2-hydroxy-naphthaldehyde-based Schiff-base. *Applied Organometallic Chemistry, 39*(3), e7900. https://doi.org/10.1002/aoc.7900.
[21] Balewski, Ł., *et al*. (2025). Synthesis, structure, and stability of copper(II) complexes containing imidazoline-phthalazine ligands with potential anticancer activity. *Pharmaceuticals, 18*(3), 375. https://doi.org/10.3390/ph18030375.
[22] Samanta, P. K., & Misra, R. (2023). Intramolecular charge transfer for optical applications. *Journal of Applied Physics, 133*(2), 025102. https://doi.org/10.1063/5.0130381.
[23] Fernandes, R. S., & Dey, N. (2022). Ion-specific bathochromic shifts: Simultaneous detection of multiple heavy metal pollutants via charge transfer interactions. *Journal of Molecular Liquids, 367*, 120369. https://doi.org/10.1016/j.molliq.2022.120369.
[24] Şahin, S. (2024). A new molecular structure and computational analyses: DFT studies, NLO properties, ADMET predictions, biological targets, and docking experiments. *Polycyclic Aromatic Compounds, 44*(6), 4029–4043. https://doi.org/10.1080/10406638.2022.2113139.
[25] Xu, J., Carney, T. E., Zhou, R., Shepard, C., & Kanai, Y. (2024). Real-time time-dependent density functional theory for simulating nonequilibrium electron dynamics. *Journal of the American Chemical Society, 146*(8), 5011–5029. https://doi.org/10.1021/jacs.3c12741.
[26] Shafiq, I., *et al.* (2025). Exploration of promising key electronic and nonlinear optical properties of bifluorenylidene based chromophores: A TD-DFT/DFT approach. *Scientific Reports, 15*(1), 10701. https://doi.org/10.1038/s41598-024-84172-y.
[27] Kateris, N., Xu, R., & Wang, H. (2023). HOMO–LUMO energy gaps of complexes of transition metals with single and multi-ring aromatics. *Combustion and Flame, 257*, 112513. https://doi.org/10.1016/j.combustflame.2022.112513.
[28] Bykov, M., Abramov, Z., Pakhomova, M., Borodina, T., Smirnov, V., & Suslov, D. (2022). Structure and catalytic properties of palladium(II)(acetylacetonato-κ²O,O′) bis(tris(diethylamino)phosphine) tetrafluoroborate. *Journal of Structural Chemistry, 63*(1), 125–139. https://doi.org/10.1134/S002247662201004X.
[29] Abdel-Baset, H. M. (2024). DFT analysis of charge distribution and electrostatic potential in SiO_2 ring clusters with different planar folds. Unpublished manuscript.
[30] Celedón, S., *et al.* (2023). Design, synthesis, solid-state and solution structures, nonlinear optical and computational studies of copper(II) complexes supported by variously substituted enantiomerically pure push–pull tetradentate Schiff base ligands. *Journal of Molecular Structure, 1293*, 136281. https://doi.org/10.1016/j.molstruc.2023.136281.
[31] Knoppe, S., Hakkinen, H., Verbiest, T., & Clays, K. (2018). Role of donor and acceptor substituents on the nonlinear optical properties of gold nanoclusters. *The Journal of Physical Chemistry C, 122*(7), 4019–4028. https://doi.org/10.1021/acs.jpcc.7b12609.
[32] Maity, S., Bain, D., & Patra, A. (2019). An overview on the current understanding of the photophysical properties of metal nanoclusters and their potential applications. *Nanoscale, 11*(47), 22685–22723. https://doi.org/10.1039/C9NR07176D.
[33] Pang, S. W., Sapari, S., Matmin, J., & Razak, F. I. A. (2020). Computational studies on nonlinear optical properties of metal complexes containing azobenzene. *Malaysian Journal of Analytical Sciences, 24*(5), 719–726.
[34] Tamer, Ö., Şimşek, M., Dege, N., Avcı, D., & Atalay, Y. (2025). The effect of complex formation on the static and frequency-dependent nonlinear optical properties: A combined experimental and theoretical investigation. *Spectrochimica Acta Part A: Molecular and Biomolecular Spectroscopy, 325*, 125138. https://doi.org/10.1016/j.saa.2024.125138.
[35] Soto, E., *et al.* (2024). $FeSi_4P_4$ and $CoSi_3P_3$: Hidden gems of ternary tetrel pnictides with outstanding nonlinear optical properties. *Chemistry of Materials, 36*(18), 8854–8863. https://doi.org/10.1021/acs.chemmater.4c02101.
[36] Kumar, R., Yadav, S. K., Seth, R., & Singh, A. (2023). Designing of gigantic first-order hyperpolarizability molecules via joining the promising organic fragments: A DFT study. *Journal of Molecular Modeling, 29*(1), 5. https://doi.org/10.1007/s00894-022-05258-4.
[37] Khairul, W. M., *et al.* (2025). The experimental and DFT approaches on electronic, thermal and conductivity properties of non-linear optical bearing fused aromatic chalcones towards prospective OLEDs. *Journal of Molecular Structure, 1319*, 139585. https://doi.org/10.1016/j.molstruc.2024.139585.
[38] Mustafa, M. N., *et al. (*2025). Elucidating the potential of nonlinear optical behavior of azo dyes for advanced laser-based technologies. *Advanced Theory and Simulations*, 2401202. https://doi.org/10.1002/adts.202401202.
[39] Habeeba, A. A. U., Saravanan, M., Girisun, T. C. S., & Anandan, S. (2021). Nonlinear optical studies of conjugated organic dyes for optical limiting applications. *Journal of Molecular Structure, 1240*, 130559.

https://doi.org/10.1016/j.molstruc.2021.130559.
[40] Sorsche, D., *et al*. (2025). Shifting the MLCT of d^6 metal complexes to the red and NIR. *Coordination Chemistry Reviews, 530*, 216454. https://doi.org/10.1016/j.ccr.2025.216454.
[41] Tariq, S., *et al.* (2024). Exploration of key electronic properties and optical nonlinearity of diamine based Schiff bases: Spectroscopic characterization and DFT study. *Journal of Molecular Structure, 1308*, 138135. https://doi.org/10.1016/j.molstruc.2023.138135.